ACS OMEGA

http://pubs.acs.org/journal/acsodf

Article

Enhanced Electrochemical Performance of the $Na_3V_2(PO_4)_3$/C Cathode Material upon Doping with Mn/Fe for Na-Ion Batteries

Yenduri Bhaskara Rao, K. Ramakrushna Achary, and Laxmi Narayana Patro*

Cite This: *ACS Omega* 2022, 7, 48192−48201

Read Online

ACCESS | Metrics & More | Article Recommendations

ABSTRACT: Research studies on Na-ion batteries (NIBs) are receiving significant scientific and commercial attention recently owing to the availability of low-cost, safe, and abundant materials in comparison to the conventional Li-ion batteries. The cathode material in a battery plays a crucial role in determining its cell capacity and cycle life. NASICON-based $Na_3V_2(PO_4)_3$, NVP, is known to be a favorable cathode material for NIBs due to its structural stability with high Na-ion mobility. The present work shows the structural and electrochemical properties of bare NVP/C and NVP/C partially doped with low-cost and much abundant transition element Fe/Mn at the toxic and expensive V site. The bare NVP/C as well as the transition-metal ion-doped NVP/C materials are prepared by the sol−gel method. XRD and FTIR studies confirm the formation of materials exhibiting the rhombohedral NVP structure ($R\bar{3}c$) without any trace of impurities. The presence of a carbon layer in the investigated cathode materials is confirmed by the HRTEM micrographs; furthermore, the oxidation states of different transition-metal elements present are evaluated by X-ray photoelectron spectroscopy. Electrochemical studies reveal that the moderate doping of Fe/Mn in NVP/C results in an enhancement in discharge capacities in the doped materials at different C rates compared to the bare NVP/C sample. The differences in their electrochemical results are explained with respect to their Na-ion diffusion coefficient values obtained using the Randles−Sevcik equation. A Mn-doped NVP/C material exhibits an enhanced discharge capacity of 107 mA h g^{-1} at 0.1C with 90% capacity retention even after 100 cycles at 1C current rate. At the end, a Na-ion full cell (NVMP/C||HC) comprising a Mn-doped NVP/C cathode with the commercial hard carbon anode delivering a discharge capacity of 90 mA h g^{-1} is demonstrated.

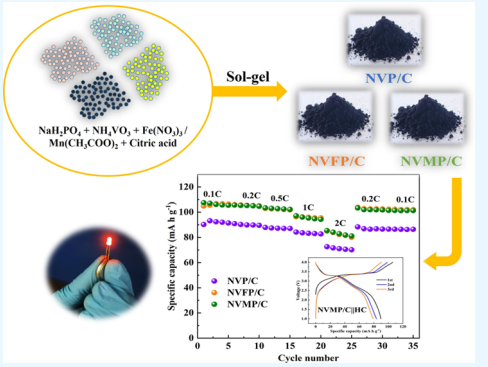

INTRODUCTION

Na-ion batteries (NIBs) find potential applications in large-scale energy-storage devices to overcome the challenges from the conventional unsafe and expensive Li-ion batteries. The materials known for NIBs are abundant, safe, and of low cost.[1−3] The cathode in a battery is the source of mobile ions determining its specific capacity, cyclability, and specific energy. A variety of layered metal oxides, polyanionic compounds, and organic materials are widely investigated as the possible cathode materials for NIBs. The metal oxides suffer from irreversible structural changes during charge/discharge cycles, whereas organic compounds often exhibit low reaction kinetics. On the other hand, polyanionic compounds offer fast Na-ion diffusion, high structural stability, high energy density, and excellent electrochemical performance.[4,5] Among the polyanionic compounds, $Na_3V_2(PO_4)_3$ (NVP) exhibits a 3D framework of NASICON (Na Super Ion CONductor, $Na_3Zr_2Si_2PO_{12}$) structure, offering larger interstitial spaces to host the Na ions upon cycling that furthermore adds a longer cycle life to the battery.[2,5] The structure of NVP (rhombohedral, $R\bar{3}c$) comprises corner-sharing VO_6 octahedra and PO_4 tetrahedra connected with the oxygen atoms (Figure 1).

There are three Na atoms distributed over two Na sites: one Na1(6b) and two Na2(18e) having sixfold and eightfold coordination with oxygen atoms, respectively.[6,7] The Na atoms present at the Na2 sites are involved actively in the charge/discharge process, whereas the Na atom present at the Na1 site is strongly bonded with the oxygen atoms. The structure of NVP is known to be stable even though the two Na atoms from the Na2 sites are stripped ($Na_3V_2(PO_4)_3 \rightarrow NaV_2(PO_4)_3$) leading to a capacity of 117.6 mA h g^{-1} because of the stronger covalent effect of $(PO_4)^{3-}$ units.[8]

One of the challenges of the NVP material development is toward the complete/partial replacement of the toxic and expensive V element with some cost-effective and abundant elements such as Fe and Mn.[9] Liu et al. showed that the stable

Received: September 28, 2022
Accepted: November 23, 2022
Published: December 15, 2022

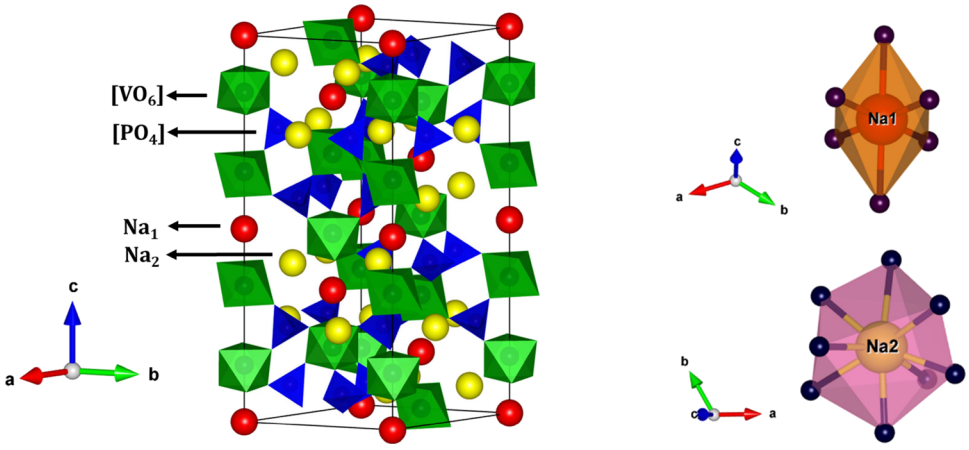

Figure 1. (a) Crystal structure of $Na_3V_2(PO_4)_3$ and (b) polyhedral view of Na1 and Na2 sites.

site for the dopant Fe in NVP is at the V site, using density functional theory calculations.[10] The presence of the multivalent transition element, V, in NVP-based materials provides the electronic conductivity and additionally promotes the chemical diffusion of Na ions. However, the large separation of VO_6 octahedral units results in lower electronic conductivity values, which is considered to be a major drawback of NVP.[11] The electronic conductivity exhibited by the cathode material often determines the rate performance of the batteries. Elemental doping and downsizing of the particles are often attempted to enhance the intrinsic electronic conductivity of NVP, whereas coating with carbon-based materials such as amorphous carbon, graphene, carbon nanotube, and so forth adds its surface electronic conductivity.[11] Various preparatory processes such as solid-state reaction, sol−gel, solvothermal, hydrothermal, and so forth are known for the synthesis of NVP-based materials. Among them, sol−gel is an effective method due to its lower operating temperature.[8] Various dopants such as Mg^{2+}, Al^{3+}, Ni^{2+}, Co^{2+}, Fe^{3+}, K^+, Mo^{6+}, and so forth of different levels using a variety of synthesis methods are used at the Na/V site of NVP to improve its electronic conductivity.[12−16] Wu et al. prepared $Na_3V_{2-x}Fe_x(PO_4)_3/C$ (x = 0.05, 0.10, and 0.15) materials modified with reduced graphene oxide (rGO) by the hydrothermal-assisted sol−gel process and reported a capacity of 91.2 mA h g^{-1} at 20C for the $Na_3V_{1.9}Fe_{0.1}(PO_4)_3/C$ + rGO sample.[17] Fang et al. reported the electrochemical behavior of $Na_3V_{2-x}Mn_x(PO_4)_3/C$ (x = 0 to 0.3) materials prepared by the freeze-drying-assisted thermal treatment method and showed the sample with x = 0.2, $Na_3V_{1.8}Mn_{0.2}(PO_4)_3/C$, delivering a capacity of 106.8 mA h g^{-1} at 1C rate.[18] Novikova et al. reported $Na_3V_{2-x}Al_x(PO_4)_3$, $Na_3V_{2-x}Fe_x(PO_4)_3$, and $Na_3V_{2-x}Cr_x(PO_4)_3$ (x = 0, 0.03, 0.05, and 0.1) materials synthesized by the sol−gel process with a capacity of 117.6 mA h g^{-1} at a discharge rate of 0.1C exhibited by the Fe (x = 0.1)-doped sample.[19]

In the present work, bare NVP/C [$Na_3V_2(PO_4)_3/C$], Mn-doped NVP/C, NVMP [$Na_3V_{1.8}Mn_{0.2}(PO_4)_3/C$], and Fe-doped NVP/C, NVFP [$Na_3V_{1.8}Fe_{0.2}(PO_4)_3/C$] materials are synthesized by the sol−gel process. The selection of the dopants, Fe and Mn, could be attributed to their high abundance, safety, and low cost in comparison to V present in NVP.[9] The current study is aimed to compare the influence of Fe/Mn on the electrochemical performance of NVP/C, keeping their doping level the same. The dopant level (x) in $Na_3V_{2-x}M_x(PO_4)_3$ (M: Mn/Fe) is fixed to 10 mol % (x = 0.2). In order to improve the surface electronic conductivity, the easily graphitizable carbon source, citric acid, is used as both the reducing and chelating agent to encapsulate the NVP particles deterring the aggregation of grains during calcination. The structural studies of bare and Mn-/Fe-doped NVP/C materials are carried out by XRD and FTIR analyses. The presence of the surface carbon layer is confirmed by HRTEM. The oxidation states of the multivalent transition-metal elements such as V and Mn/Fe are determined by XPS. At the end, the electrochemical performances of the cathode materials are tested by galvanostatic and potentiostatic methods.

EXPERIMENTAL METHODS

Material Synthesis. Cathode materials with nominal stoichiometry $Na_3V_2(PO_4)_3/C$ [NVP/C], $Na_3V_{1.8}Fe_{0.2}(PO_4)_3/C$ [NVFP/C], and $Na_3V_{1.8}Mn_{0.2}(PO_4)_3/C$ [NVMP/C] were prepared by the sol−gel process. Initially, the stoichiometric quantities of NaH_2PO_4, NH_4VO_3, $Fe(NO_3)_3{\cdot}9H_2O$/$Mn(CH_3COO)_2$, and citric acid were mixed in DI water. The solution was then stirred for 4 h at 80 °C until a gel was developed; later, the gel was vacuum-dried at 120 °C. The ground product was preheated for 4 h at 350 °C under air atmosphere, followed by calcination at 700 °C for 8 h in the N_2 atmosphere. Citric acid used as the carbon source that additionally acts as a reducing agent, reducing V from its V^{5+} (NH_4VO_3) to V^{3+} (NVP) state. It is to be noted here that the oxidation states of Fe and Mn corresponding to their initial precursors, $Fe(NO_3)_3{\cdot}9H_2O$ and $Mn(CH_3COO)_2$, are +3 and +2, respectively.

Material Characterization. The XRD patterns of the cathode materials were recorded using an X-ray diffractometer (PANalytical Empyrean) with Cu−Kα radiation. The samples were scanned in the 2θ window of 10°−90° at a step size of 0.01313. High-Score plus software is used for the Rietveld refinement analysis. The presence of various functional groups such as PO_4 tetrahedra and VO_6 octahedra was confirmed by FTIR spectroscopy using a Bruker FTIR spectrometer. The nature of carbon present in the carbon layers was investigated by Raman spectroscopy (HORIBA, France). The microstructural features of the carbon-coated NVP-based materials were obtained using a HRTEM system (JEOL-JEM 2100). The oxidation states of different transition elements such as V,

https://doi.org/10.1021/acsomega.2c06261
ACS Omega 2022, 7, 48192−48201

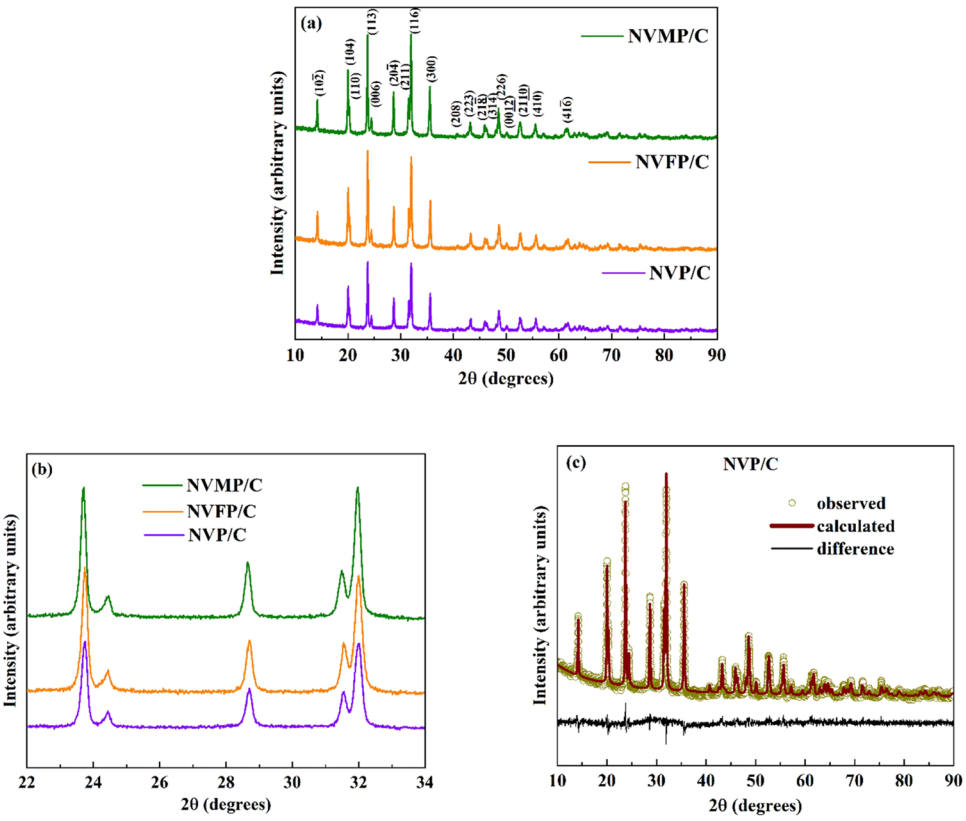

Figure 2. (a) XRD patterns of NVP/C, NVFP/C, and NVMP/C materials; (b) enlarged view of the (1 1 3), (2 0 $\bar{4}$),and (1 1 6) peaks; and (c) observed and calculated XRD patterns of NVP/C.

Fe, and Mn present were obtained by using an XPS instrument (ULVAC − PHI5000).

Electrochemical Characterization. The electrochemical tests were performed using CR2032-type coin cells assembled in an Ar-filled glovebox, with the H_2O and O_2 levels below 0.1 ppm. The electrodes were prepared by mixing the active material, carbon black, and polyvinylidene fluoride (PVDF) binder in the weight ratio of 80:10:10 in *N*-methyl-2-pyrrolidone (NMP) solvent. The mixed slurry was initially spread onto an aluminum foil serving as a current collector and then dried at 100 °C in a vacuum overnight to evaporate the solvent. The average loading mass of the active material was approximately 3−4 mg cm^{-2}. A glass microfiber filter (Whatman, Grade GF/F) was used as the separator, whereas 1 M $NaClO_4$ in EC (ethylene carbonate) and PC (propylene carbonate) at 1:1 v/v was used as the electrolyte. The electrochemical measurements were carried out using a Na metal foil as the counter/reference electrode. Cyclic voltammetry (CV) curves at different scan rates were recorded using Metrohm Autolab to evaluate the reversibility of the redox reactions. The galvanostatic charge/discharge studies were done in the voltage window of 2−4 V (vs Na^+/Na) at various C rates using Neware BTS-610. Impedance measurements in the frequency range of 10 kHz to 10 mHz were carried out at the fully charged state (4.0 V) using Metrohm Autolab. All the electrochemical measurements were done at room temperature.

At the end, a coin-type (CR2032) Na-ion full cell was constructed using the NVP-based cathode material exhibiting the best electrochemical characteristics along with the presodiated hard carbon as the anode. In the present study, commercial hard carbon was used. The presodiation of hard carbon was performed prior to the fabrication of the full cell. The capacity balancing of the full cell was maintained with the active loading mass ratio of the cathode and anode as 3:1. $NaClO_4$ (1 M) in a mixture of EC and PC (1:1 v/v) and a glass microfiber filter were employed as the electrolyte and separator, respectively.

RESULTS AND DISCUSSION

The powder XRD patterns of bare NVP/C, NVFP/C, and NVMP/C materials are displayed in Figure 2. In all cases, the

Table 1. Structural Details of NVP/C, NVFP/C, and NVMP/C Materials Taken from the Rietveld Refinement

sample	a (= b) (Å)	c (Å)	V(Å^3)	χ^2 (GoF)
NVP/C	8.725(3)	21.825(2)	1438.92(0)	1.2
NVFP/C	8.726(0)	21.823(3)	1439.02(6)	1.3
NVMP/C	8.738(2)	21.821(1)	1442.90(7)	1.1

diffraction peaks agree well with the rhombohedral NASICON, NVP structure ($R\bar{3}C$). The absence of an additional peak indicates that the doping of 10 mol % Fe/Mn in NVP/C does not alter its crystal structure. In addition, no peaks corresponding to carbon appeared, confirming its amorphous nature. The extension of broadening is the same in all the cases, indicating similar crystallite sizes.

It is evident from Figure 2 that the peaks in the NVMP/C sample are shifted to a lower angle side, which is related to the larger ionic radius of Mn^{2+} as compared to that of V^{3+}.[20] Nevertheless, this tendency is not observed much clearly for the NVFP/C material as the ionic radii of Fe^{3+} and V^{3+} are

https://doi.org/10.1021/acsomega.2c06261
ACS Omega 2022, 7, 48192−48201

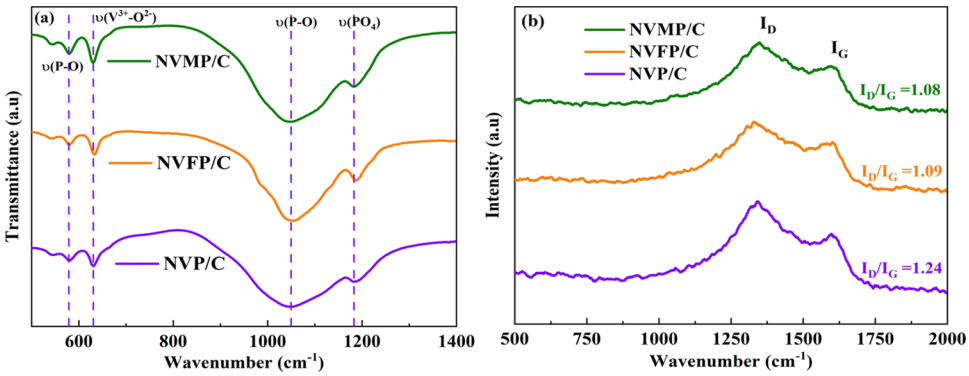

Figure 3. (a) FTIR and (b) Raman spectra of NVP/C, NVFP/C, and NVMP/C materials.

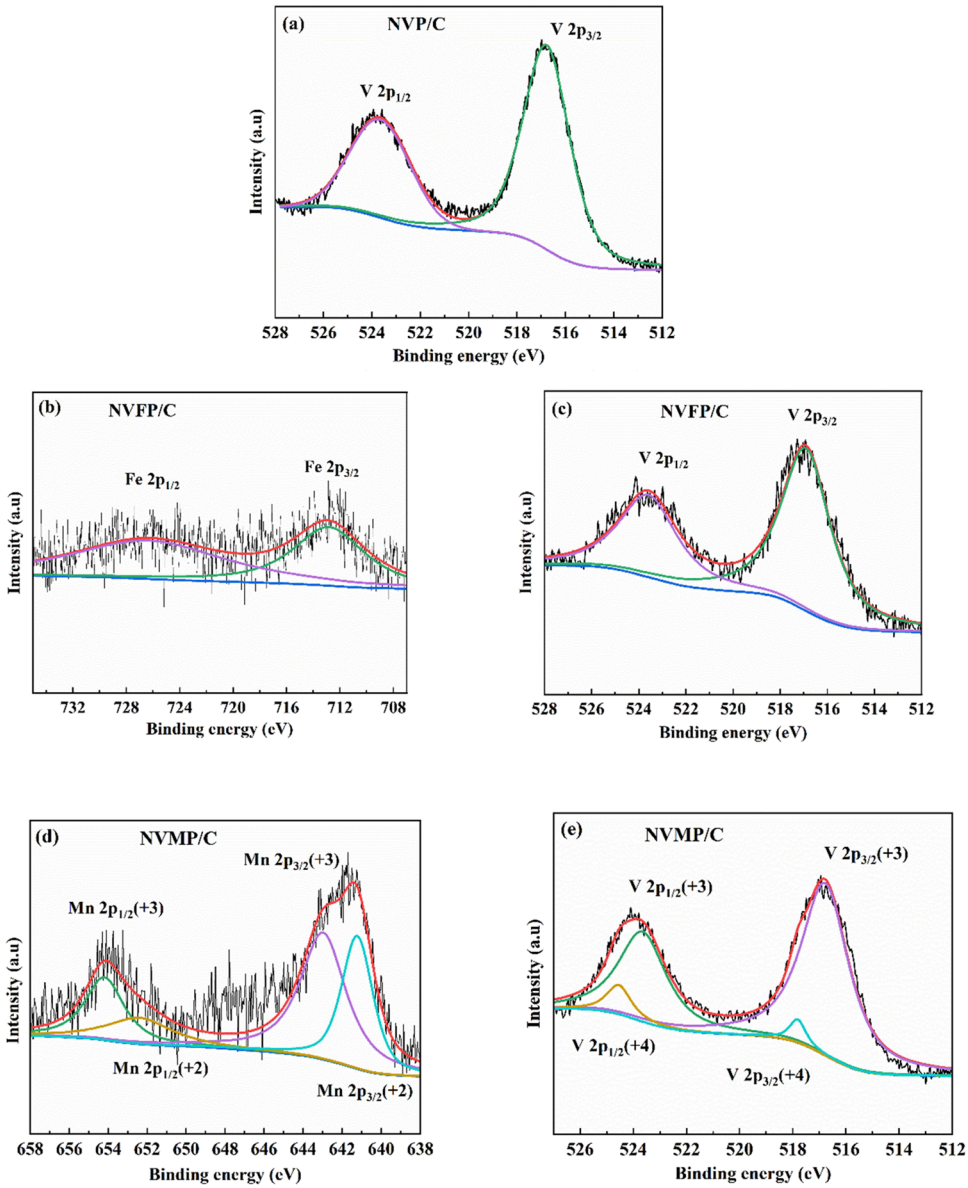

Figure 4. XPS spectra of (a) V 2p in NVP/C, (b) Fe 2p in NVFP/C, (c) V 2p in NVFP/C, (d) Mn 2p in NVMP/C, and (e) V 2p in NVMP/C materials.

quite similar.[14] Further, Rietveld refinements are performed to elucidate the influence of Fe/Mn doping on the structural parameters of NVP/C. The lattice parameters of NVP/C, NVFP/C, and NVMP/C are summarized in Table 1. The doping of Mn at V site clearly results in an increment in a (= b) axis and unit cell volume. However, the increment in unit cell volume is minimal when Fe replaces V.

https://doi.org/10.1021/acsomega.2c06261
ACS Omega 2022, 7, 48192−48201

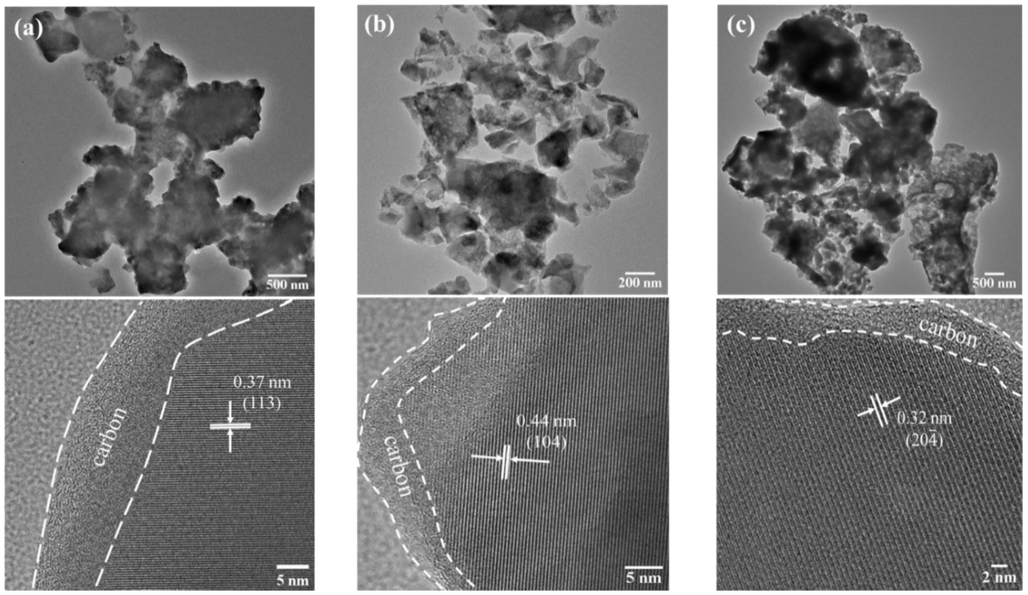

Figure 5. HRTEM images of (a) NVP/C, (b) NVFP/C, and (c) NVMP/C materials.

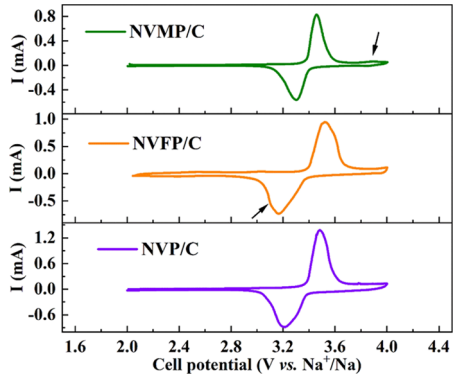

Figure 6. Cyclic voltammetry profiles of cells with NVP/C, NVFP/C, and NVMP/C electrodes recorded at a scan rate of 0.1 mV s^{-1}.

Figure 3a shows the FTIR spectra of NVP/C, NVFP/C, and NVMP/C materials. The bands observed at ~579 and ~1050 cm^{-1} are attributed to the presence of P−O bonds in PO_4 tetrahedra. The stretching vibration of the terminal PO_4 units is observed in the range of ~1150 to 1250 cm^{-1}. The band detected at ~631 cm^{-1} corresponds to the vibration of V^{3+}−O^{2-} bonds in the isolated VO_6 octahedra.[21] Moreover, there are no bands observed with respect to the occurrence of V^{5+}−O^{2-} in the as-prepared materials. This clearly shows the complete reduction of raw V^{5+} into V^{3+} in all the NVP/C, NVFP/C, and NVMP/C samples.[22]

Figure 3b shows the Raman spectra of NVP/C, NVFP/C, and NVMP/C materials. Two characteristic peaks are observed at ~1340 and ~1600 cm^{-1}, corresponding to the disordered (D) and graphitic (G) carbon regions, respectively. The intensity ratio of the D and G bands (I_D/I_G ratio) is the critical parameter to evaluate the character of carbon materials with disordered and graphitic nature. Here, the calculated I_D/I_G ratios are found to be 1.08, 1.09, and 1.24 for NVMP/C, NVFP/C, and NVP/C materials, respectively. It is seen that the graphitic carbon content is increased for Fe- and Mn-doped NVP/C materials compared to that of undoped NVP/C, indicating higher electronic conductivity in the doped materials.[10]

The valence states of the transition-metal elements, V, Fe, and Mn in NVP/C, NVFP/C, and NVMP/C samples are determined by XPS (Figure 4). In the case of NVP/C, the binding energy values observed at ~516.7 and 523.6 eV from the V 2p XPS spectra are, respectively, attributed to $2p_{3/2}$ and $2p_{1/2}$ transitions, confirming the oxidation state of V as +3 (Figure 4a). In the case of NVFP/C, the peaks observed at ~712.8 and 726.3 eV are assigned to $2p_{3/2}$ and $2p_{1/2}$ transitions of Fe^{3+} (Figure 4b) in accordance with the previous reports.[10] It is also seen that the oxidation state of V (+3) is not altered after doping Fe (+3) in NVP/C (Figure 4c).

In the case of NVMP/C, the peaks observed at ~642.9 and ~654.1 eV belong to Mn^{3+}, while the peaks observed at ~641.2 and ~652.3 eV belong to Mn^{2+} (Figure 4d), indicating the coexistence of both Mn^{2+} and Mn^{3+} in the NVMP/C sample.[18] As a result, two more V 2p peaks at ~517.8 and ~524.4 eV are observed in addition to the valence state of V^{3+} in the NVMP/C sample (Figure 4e), showing V at its both +4 and +3 oxidation states. However, the signature of V^{4+} is not observed in the NVFP/C sample (Figure 4c). In NVMP/C, the presence of V in the +4 oxidation state is mainly to compensate the charge imbalance created by the difference in the valence state of the host V^{3+} and dopant Mn^{2+} ions.

The microscopic features of the active material and the carbon layer present on its surface are observed by using HRTEM (Figure 5). The doped materials show irregular shapes of sizes with less agglomeration compared to that of bare NVP/C.

In all cases, the presence of a carbon coating layer on the surface of the encapsulated particles is clearly seen, and the average thickness of the carbon layer for the doped samples NVFP/C and NVMP/C is found to be ~4 nm, which is narrower compared to that of the bare NVP/C sample (~10 nm). The interplanar spacing calculated from the lattice fringes is well consistent with the corresponding (*h k l*) plane of the rhombohedral NVP phase shown in Figure 2.

The CV curves in the voltage range of 2−4 V are recorded at a scan rate of 0.1 mV s^{-1} for the cells with NVP/C, NVFP/C, and NVMP/C electrodes (Figure 6) to understand their electrochemical behavior. Sharp oxidation and reduction peaks

https://doi.org/10.1021/acsomega.2c06261
ACS Omega 2022, 7, 48192−48201

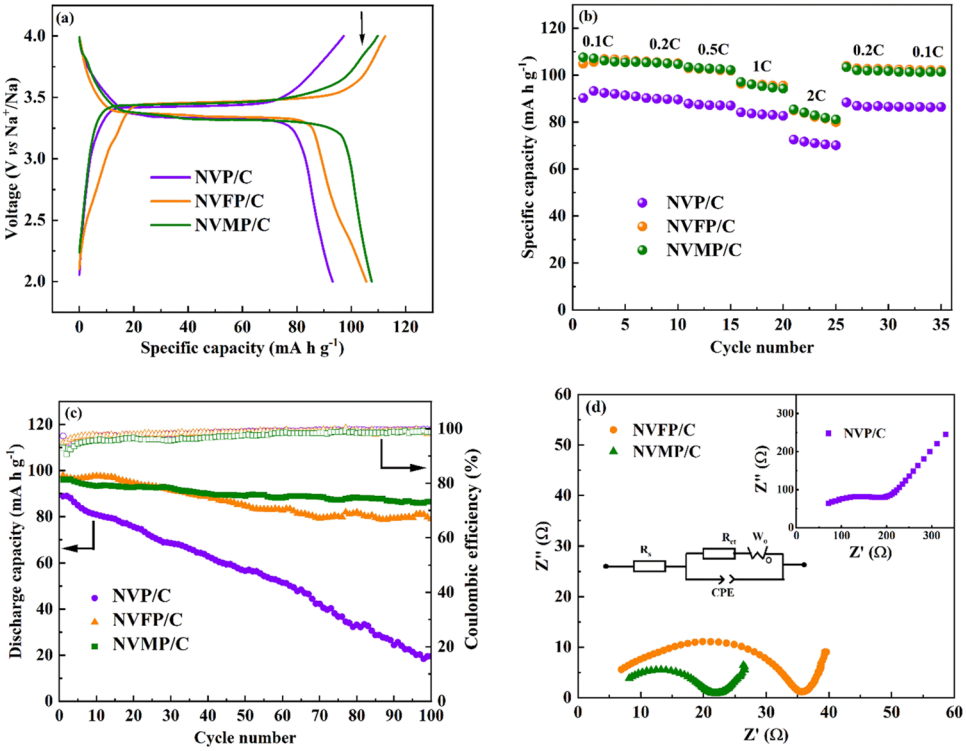

Figure 7. (a) Initial charge−discharge profile at 0.1C, (b) rate capability, (c) cycling stability at 1C, and (d) Nyquist impedance plots of the cells (at the fully charged state, 4.0 V) with NVP/C, NVFP/C, and NVMP/C electrodes.

are observed for the bare NVP/C sample at 3.48 and 3.21 V, indicating the extraction and insertion of Na ions during charging and discharging, respectively.[14] No additional peaks are observed, indicating the absence of any further reactions in the cell. In the NVFP/C electrode, the oxidation and reduction peaks are slightly shifted to a higher voltage (3.52 V) on charging and a lower voltage (3.16 V) on discharging, respectively. This could be attributed to the change in ionicity of V^{3+} when it is partially replaced with Fe^{3+}.[14]

It is worth to note here that a small broad reduction peak at approximately ∼3.1 V is observed, indicating a two-step transformation of Na ions during the discharging process, in accordance with the literature.[10] In the case of the NVMP/C electrode, along with the main redox peak at ∼3.4 V, another small reversible redox peak is observed at ∼3.9 V (Figure 6), indicating the extraction of a third Na atom related to the V^{4+}/V^{5+} redox couple after the substitution of Mn^{2+} at the V^{3+}site.[23]

The electrochemical performance of the cells with bare NVP/C and Fe-/Mn-doped NVP/C samples is evaluated. Figure 7a presents the first charge−discharge profiles of the cells cycled at 0.1C showing a long voltage plateau approximately at 3.4 V associated with the extraction and insertion of Na ions ($V^{3+/4+}$ redox couple). In NVMP/C, another small voltage plateau close to 3.9 V is observed in line with the CV results shown in Figure 6. The first charge capacities exhibited by the bare NVP/C, NVFP/C, and NVMP/C electrodes are 97, 112, and 109 mA h g^{-1}, respectively, whereas the first discharge capacities are 93, 105, and 107 mA h g^{-1}, respectively. The rate performances of the cells with bare NVP/C, NVFP/C, and NVMP/C are studied from 0.1C to 2C rates and eventually decreasing again to 0.1C rate (Figure 7b). The bare NVP/C sample displays the discharge capacities of 93, 90, 87, 84, and 72 mA h g^{-1}, while the NVFP/C sample shows the discharge capacities of 106, 105, 102, 96, and 84 at 0.1C, 0.2C, 0.5C, 1C, and 2C, respectively. Further, the discharge capacities of 107, 105, 103, 97, and 84 mA h g^{-1} at 0.1C, 0.2C, 0.5C, 1C, and 2C, respectively, are observed for the NVMP/C sample. It is observed that the discharge capacities exhibited by the Fe-/Mn-doped NVP/C samples are similar at different C rates and higher than those from the cell with the bare NVP/C electrode. Additionally, the discharge capacities of all the materials reached nearly their original values at 0.1C rate even after applying to 2C rate.

Figure 7c shows the cyclic performance of the cells with NVP/C, NVFP/C, and NVMP/C electrodes at 1C rate. The NVMP/C material shows an initial discharge capacity of 96 mA h g^{-1} and retains a capacity of 86 mA h g^{-1} after 100 cycles with a capacity retention of 90%. On the other side, NVFP/C delivers a discharge capacity of 79 mA h g^{-1} with a capacity retention of 81% after 100 cycles. However bare NVP/C delivers a low capacity of 20 mA h g^{-1} after 100 cycles with a capacity retention of only 22%. Coulombic efficiency of more than 98% is observed in all the cases. The electrochemical results thus confirmed better cyclic performances of the cells with the doped materials compared to the bare one.

The superior electrochemical performance observed in Fe-/Mn-doped NVP materials is further explained with respect to their Nyquist impedance plots measured at their fully charged state (Figure 7d). The impedance plot consists of a semicircle in the high-frequency region, followed by a small straight line in the low-frequency region, indicating that the electrochemical process is controlled by both charge transfer and ion diffusion. In the equivalent circuit, R_s and R_{ct}, respectively, correspond to the electrolyte resistance and charge-transfer resistance, whereas CPE and Wo represent the double-layer capacitance and Warburg impedance, respectively.[20] Notably, Fe- and Mn-doped NVP/C materials exhibit lower charge-transfer

https://doi.org/10.1021/acsomega.2c06261
ACS Omega 2022, 7, 48192−48201

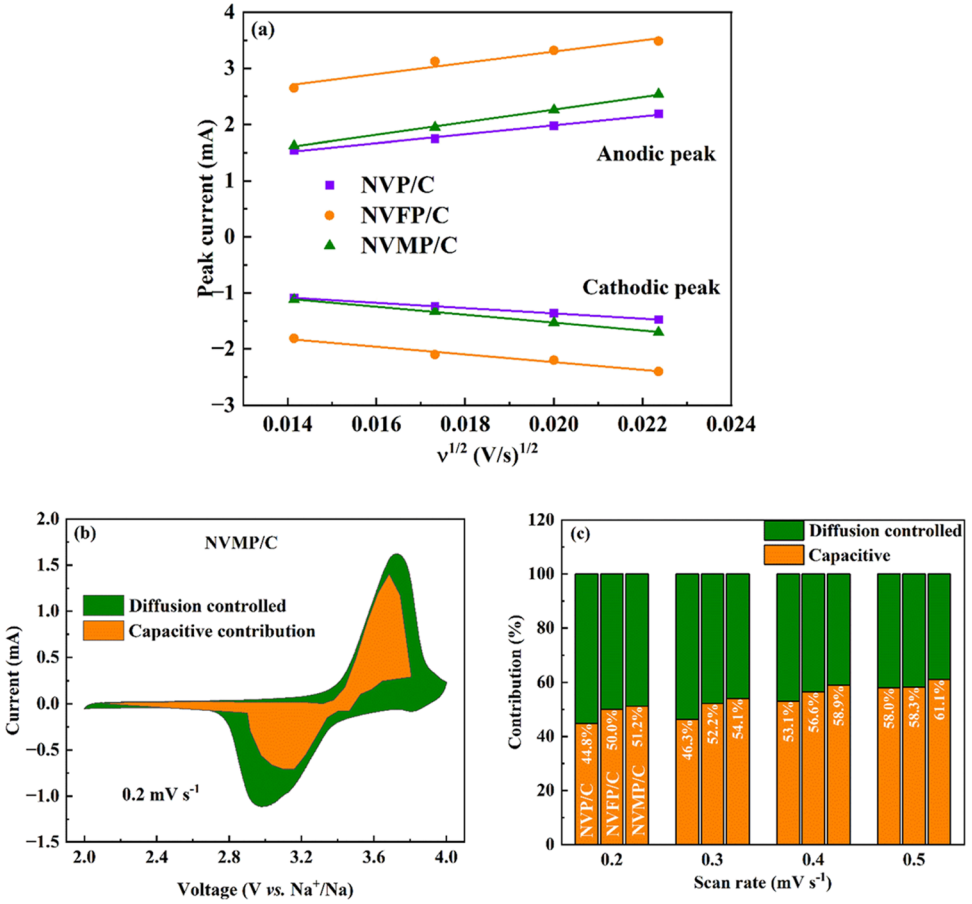

Figure 8. (a) Relationship of i_p with $\nu^{1/2}$. (b) CV curve of the NVMP/C material showing the diffusion-controlled and capacitive contributions at a scan rate of 0.2 mV s^{-1}. (c) Comparison of the calculated diffusion-controlled and capacitive contributions to the total capacity of NVP/C, NVFP/C, and NVMP/C electrodes at different scan rates.

Table 2. Calculated Diffusion Coefficients (D_{Na}) of Na Ions in the NVP/C, NVFP/C, and NVMP/C Electrodes

	diffusion coefficient, D_{Na}(cm^2 s^{-1})	
sample name	anodic	cathodic
NVP/C	3.497×10^{-11}	1.230×10^{-11}
NVFP/C	5.603×10^{-11}	2.628×10^{-11}
NVMP/C	6.950×10^{-11}	2.799×10^{-11}

resistance (R_{ct}) values of 31 and 17 Ω, respectively, in comparison to that of the bare NVP material (150 Ω), confirming better charge transfer at the electrolyte−electrode interface and improved electrochemical performance in the doped systems.

In order to explain the differences in their cyclic performances, the diffusion kinetics of Na ions are studied by measuring their CV curves at different scan rates, ranging from 0.2 to 0.5 mV s^{-1} (Figure 8a).

The diffusion coefficient of Na ions (D_{Na}) at room temperature is determined from the Randles−Sevcik equation[18]

$$i_p = 2.69 \times 10^5 n^{3/2} A {D_{Na}}^{1/2} C_{Na} \nu^{1/2} \quad (1)$$

Here i_p is the peak current, A is the electrode surface area, C_{Na} is the molar concentration of Na ions in the cathode material, n is the number of transferred electrons (n = 2 for the V^{3+}/V^{4+} redox couple), and ν is the scan rate. The D_{Na} values of the anodic and cathodic processes are given in Table 2.

The doped materials, NVFP/C and NVMP/C, have the largest Na ion diffusion coefficient values, and they are in agreement with the literature.[24−26] The appropriate doping of Mn/Fe ions at the V site of NVP/C thus enlarges the transportation channels, reducing the migration barriers due to which the Na ions could easily be transported.

The diffusive and capacitive contributions to the total capacity can be calculated by analyzing the total response current at a fixed potential, V. It is well known that the response current, i, varies linearly with the scan rate, ν, when the current is provided by the surface reactions, whereas the current is dominated by diffusion when the response current varies linearly with $\nu^{1/2}$. The total current consisting of surface-capacitive ($k_1\nu$) and diffusion-controlled ($k_2\nu^{1/2}$) processes can be expressed by the following equation[27]

$$i(V) = k_1\nu + k_2\nu^{1/2} \text{ or } \frac{i(V)}{\nu^{1/2}} = k_1\nu^{1/2} + k_2 \quad (2)$$

The constants k_1 and k_2 can be evaluated, respectively, from the slope and intercept of the linear plot between $\frac{i(V)}{\nu^{1/2}}$ and $\nu^{1/2}$. Figure 8b shows the surface-capacitive (shaded in orange) and diffusion-controlled (shaded in olive) contributions to the CV plot of the NVMP/C material at a scan rate of 0.2 mV s^{-1}. The capacitive and diffusion-controlled contributions to the total

https://doi.org/10.1021/acsomega.2c06261
ACS Omega 2022, 7, 48192−48201

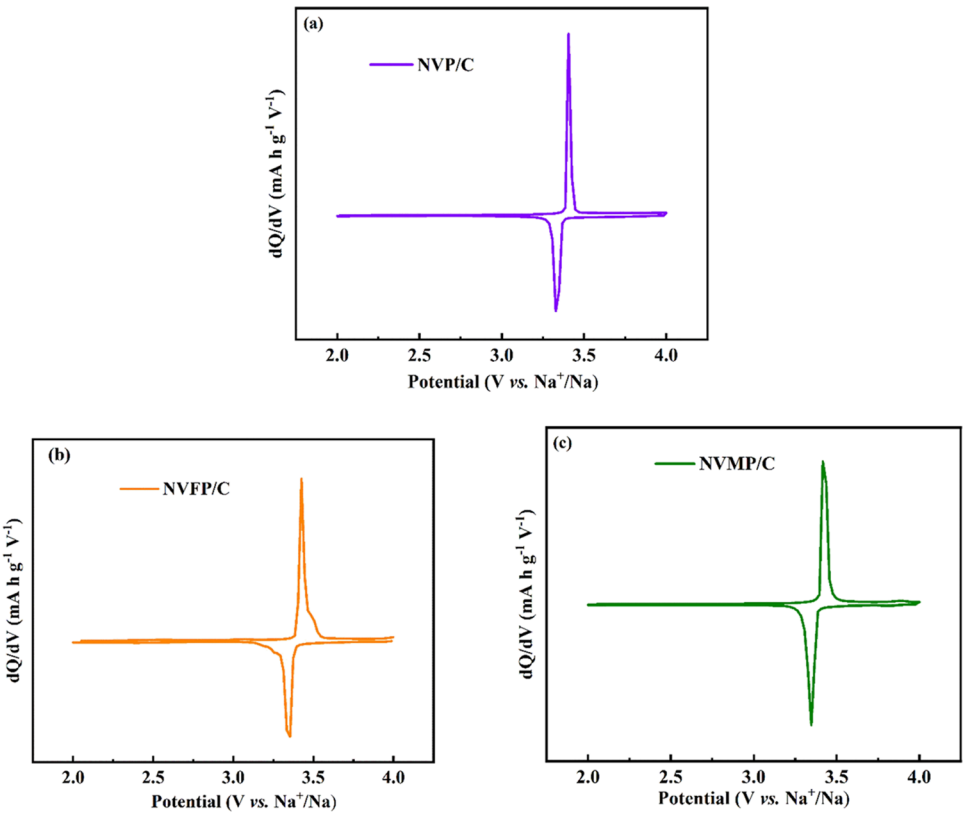

Figure 9. dQ/dV curves at 0.1C for the second cycle of the cells with (a) NVP/C, (b) NVFP/C, and (c) NVMP/C electrodes.

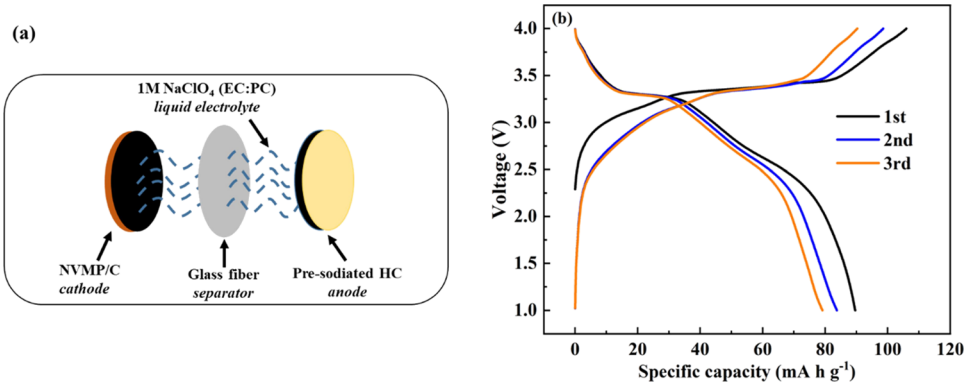

Figure 10. (a) Schematic diagram of the NVMP/C||HC full cell. (b) Charge−discharge profiles of the NVMP/C||HC full cell at 0.1C.

capacity for the NVP/C, NVFP/C, and NVMP/C electrodes on the CV plots at different scan rates (0.2−0.5 mV s^{-1}) are shown in Figure 8c. The capacitive contributions to the total capacity are higher in the Mn- and Fe-doped NVP/C systems, indicating better kinetics in the doped electrode materials.[28]

The internal charge/discharge plateau (ΔV) values from the $\frac{dQ}{dV}$ curves (differential capacitive) illustrated in Figure 9 are found to be 0.078, 0.071, and 0.070 V for the cells with NVP/C, NVFP/C, and NVMP/C electrodes, respectively. The smaller ΔV values found for the Fe-/Mn-doped NVP/C samples compared to that of the bare NVP/C sample further support their better rate performance.[10] Although both the doped systems exhibit similar electrochemical characteristics, NVMP/C shows good cyclic performances.

At the end, a Na-ion full cell is fabricated by coupling the best performing cathode NVMP/C with the presodiated hard carbon (HC) anode and tested in the voltage window of 1−4 V at 0.1C. Various anode materials such as metal oxides, sulfides, metal−alloys, and carbonaceous materials are known in the literature for Na-ion battery applications.[29] Among them, hard carbon is advantageous due to its lower operating potential and higher cation storage capacity. The schematic representation of the NVMP/C||HC full cell and its first three charge−discharge cycles are shown in Figure 10. The full cell delivers an initial discharge capacity of 90 mA h g^{-1} with an average working voltage of 3.3 V. An overall energy density of 210 Wh kg^{-1} is obtained based on the active mass of the anode and cathode materials. The electrochemical result of the full cell further shows the suitability of the Mn-doped NVP material as a potential cathode material for Na-ion batteries.

https://doi.org/10.1021/acsomega.2c06261
ACS Omega 2022, 7, 48192−48201

CONCLUSIONS

Bare NVP/C and Fe-/Mn-doped NVP/C materials are successfully prepared by the sol−gel method. XRD results confirmed the formation of the doped materials with a rhombohedral NVP structure. Encapsulation of the cathode material by carbon coating is observed through HRTEM micrographs. Improved rate performance and cyclic stability are observed by the cells with the Fe-/Mn-doped samples, NVFP/C and NVMP/C, in comparison to the bare NVP/C. The unit cell volume increases after doping Mn in NVP. However, the unit cell volume does not change much in the Fe-doped NVP system due to the similar ionic radii of Fe and V. The present analysis concludes that the enhanced electrochemical characteristics of the doped systems are also related to the ionicity of the dopant element. Although similar rate performance is observed by both the doped systems, the NVMP/C sample showed an enhanced cycling stability, delivering a high discharge capacity of 86 mA h g^{-1} even after 100 cycles at 1C with a capacity retention of 90%. Furthermore, the electrochemical results of the NVMP/C||HC Na-ion full cell shows the first discharge capacity of 90 mA h g^{-1}, with the energy density close to 210 Wh kg^{-1}. The present investigation shows that a moderate replacement of the high-cost and toxic element, *V*, with the low-cost and environmentally safe elements Fe/Mn in the NVP/C structure not only reduces the cost of the material but also enhances its electrochemical performance. The electrochemical studies on both the half and full cells employing the NVMP/C electrode show its feasibility to be used as a potential cathode material for the low-cost rechargeable Na-ion batteries.

AUTHOR INFORMATION

Corresponding Author

Laxmi Narayana Patro − *Department of Physics and SRM-Amara Raja Centre for Energy Storage Devices, SRM University AP, Amaravati, Andhra Pradesh 522502, India;* orcid.org/0000-0002-3942-6733; Phone: 0863-2343000; Email: laxminarayana.p@srmap.edu.in, patrolng@gmail.com; Fax: 0863-2343111

Authors

Yenduri Bhaskara Rao − *Department of Physics and SRM-Amara Raja Centre for Energy Storage Devices, SRM University AP, Amaravati, Andhra Pradesh 522502, India;* orcid.org/0000-0001-5984-752X

K. Ramakrushna Achary − *Department of Physics and SRM-Amara Raja Centre for Energy Storage Devices, SRM University AP, Amaravati, Andhra Pradesh 522502, India*

Complete contact information is available at: https://pubs.acs.org/10.1021/acsomega.2c06261

Notes

The authors declare no competing financial interest.

ACKNOWLEDGMENTS

Dr. L. N. Patro and K. Ramakrushna Achary acknowledge DST-SERB (Grant Number: SRG/2019/000767) for the funding.

REFERENCES

(1) Yabuuchi, N.; Kubota, K.; Dahbi, M.; Komaba, S. Research development on sodium-ion batteries. *Chem. Rev.* **2014**, *114*, 11636−11682.

(2) Zhang, X.; Rui, X.; Chen, D.; Tan, H.; Yang, D.; Huang, S.; Yu, Y. $Na_3V_2(PO_4)_3$: An advanced cathode for sodium-ion batteries. *Nanoscale* **2019**, *11*, 2556−2576.

(3) Rao, Y. B.; Bharathi, K. K.; Patro, L. N. Review on the synthesis and doping strategies in enhancing the Na ion conductivity of $Na_3Zr_2Si_2PO_{12}$ (NASICON) based solid electrolytes. *Solid State Ionics* **2021**, *366-367*, No. 115671.

(4) Hwang, J. Y.; Myung, S. T.; Sun, Y. K. Sodium-ion batteries: Present and future. *Chem. Soc. Rev.* **2017**, *46*, 3529−3614.

(5) Lyu, Y.; Liu, Y.; Yu, Z. E.; Su, N.; Liu, Y.; Li, W.; Li, Q.; Guo, B.; Liu, B. Recent advances in high energy-density cathode materials for sodium-ion batteries. *Sustain. Mater. Technol.* **2019**, *21*, No. e00098.

(6) Wei, C.; Luo, F.; Zhang, C.; Gao, H.; Niu, J.; Ma, W.; Bai, Y.; Zhang, Z. Voltage window-dependent electrochemical performance and reaction mechanisms of $Na_3V_2(PO_4)_3$ cathode for high-capacity sodium ion batteries. *Ionics* **2020**, *26*, 2343−2351.

(7) Wang, Q.; Zhang, M.; Zhou, C.; Chen, Y. Concerted ion-exchange mechanism for sodium diffusion and its promotion in $Na_3V_2(PO_4)_3$ framework. *J. Phys. Chem. C* **2018**, *122*, 16649−16654.

(8) Zeng, X.; Peng, J.; Guo, Y.; Zhu, H.; Huang, X. Research progress on $Na_3V_2(PO_4)_3$ cathode material of sodium ion battery. *Front. Chem.* **2020**, *8*, 635.

(9) Chen, M.; Liu, Q.; Wang, S. W.; Wang, E.; Guo, X.; Chou, S. L. High-abundance and low-cost metal-based cathode materials for sodium-ion batteries: Problems, progress, and key technologies. *Adv. Energy Mater.* **2019**, *9*, No. 1803609.

(10) Liu, X.; Feng, G.; Wang, E.; Chen, H.; Wu, Z.; Xiang, W.; Zhong, Y.; Chen, Y.; Guo, X.; Zhong, B. Insight into preparation of Fe-doped $Na_3V_2(PO_4)_3$@C from aspects of particle morphology design, crystal structure modulation, and carbon graphitization regulation. *ACS Appl. Mater. Interfaces* **2019**, *11*, 12421−12430.

(11) Zheng, Q.; Yi, H.; Li, X.; Zhang, H. Progress and prospect for NASICON-type $Na_3V_2(PO_4)_3$ for electrochemical energy storage. *J. Energy Chem.* **2018**, *27*, 1597−1617.

(12) Bag, S.; Murarka, H.; Zhou, C.; Bhattacharya, A.; Jokhakar, D.; Pol, V. G.; Thangadurai, V. Understanding the Na-ion storage mechanism in $Na_{3+x}V_{2-x}M_x(PO_4)_3$ (M = Ni^{2+}, Co^{2+}, $Mg^{2+}x$ = 0.1-0.5) cathodes. *ACS Appl. Energy Mater.* **2020**, *3*, 8475−8486.

(13) Wu, C.; Tong, J.; Gao, J.; Li, J.; Li, X.; Zhu, J.; Gu, M.; Zhou, W. Studies on the sodium storage performances of $Na_3Al_xV_{2-x}(PO_4)_3$@C composites from calculations and experimental analysis. *ACS Appl. Energy Mater.* **2021**, *4*, 1120−1129.

(14) Aragón, M. J.; Lavela, P.; Ortiz, G. F.; Tirado, J. L. Effect of iron substitution in the electrochemical performance of $Na_3V_2(PO_4)_3$ as cathode for Na-ion batteries. *J. Electrochem. Soc.* **2015**, *162*, A3077−A3083.

(15) Lim, S. J.; Han, D. W.; Nam, D. H.; Hong, K. S.; Eom, J. Y.; Ryu, W. H.; Kwon, H. S. Structural enhancement of $Na_3V_2(PO_4)_3$/C composite cathode materials by pillar ion doping for high power and long cycle life sodium-ion batteries. *J. Mater. Chem. A* **2014**, *2*, 19623−19632.

(16) Li, X.; Huang, Y.; Wang, J.; Miao, L.; Li, Y.; Liu, Y.; Qiu, Y.; Fang, C.; Han, J.; Huang, Y. High valence Mo-doped $Na_3V_2(PO_4)_3$/C as a high rate and stable cycle-life cathode for sodium battery. *J. Mater. Chem. A* **2018**, *6*, 1390−1396.

(17) Wu, T.; Sun, J.; Yap, Z. Q. J.; Ke, M.; Lim, C. Y. H.; Lu, L. Substantial doping engineering in $Na_3V_{2-x}Fe_x(PO_4)_3$ ($0 \le x \le 0.15$) as high-rate cathode for sodium-ion battery. *Mater. Des.* **2020**, *186*, No. 108287.

(18) Fang, J.; Wang, S.; Yao, X.; Hu, X.; Wang, Y.; Wang, H. Ration design of porous Mn-doped $Na_3V_2(PO_4)_3$ cathode for high rate and super stable sodium-ion batteries. *Electrochim. Acta* **2019**, *295*, 262−269.

(19) Novikova, S. A.; Larkovich, R. V.; Chekannikov, A. A.; Kulova, T. L.; Skundin, A. M.; Yaroslavtsev, A. B. Electrical conductivity and

https://doi.org/10.1021/acsomega.2c06261
ACS Omega 2022, 7, 48192−48201

electrochemical characteristics of $Na_3V_2(PO_4)_3$-based NASICON-type materials. *Inorg. Mater.* **2018**, *54*, 794−804.
(20) Shen, W.; Li, H.; Guo, Z.; Li, Z.; Xu, Q.; Liu, H.; Wang, Y. Improvement on the high-rate performance of Mn-doped $Na_3V_2(PO_4)_3$/C as a cathode material for sodium ion batteries. *RSC Adv.* **2016**, *6*, 71581−71588.
(21) Lim, S. Y.; Kim, H.; Shakoor, R. A.; Jung, Y.; Choi, J. W. Electrochemical and thermal properties of NASICON structured $Na_3V_2(PO_4)_3$ as a sodium rechargeable battery cathode: A combined experimental and theoretical study. *J. Electrochem. Soc.* **2012**, *159*, A1393−A1397.
(22) Song, W.; Cao, X.; Wu, Z.; Chen, J.; Huangfu, K.; Wang, X.; Huang, Y.; Ji, X. A study into the extracted ion number for NASICON structured $Na_3V_2(PO_4)_3$ in sodium-ion batteries. *Phys. Chem. Chem. Phys.* **2014**, *16*, 17681−17687.
(23) Zhang, J.; Zhao, X.; Song, Y.; Li, Q.; Liu, Y.; Chen, J.; Xing, X. Understanding the superior sodium-ion storage in a novel $Na_{3.5}Mn_{0.5}V_{1.5}(PO_4)_3$ cathode. *Energy Storage Mater.* **2019**, *23*, 25−34.
(24) Wang, H.; Jiang, D.; Zhang, Y.; Li, G.; Lan, X.; Zhong, H.; Zhang, Z.; Jiang, Y. Self-combustion synthesis of $Na_3V_2(PO_4)_3$ nanoparticles coated with carbon shell as cathode materials for sodium-ion batteries. *Electrochim. Acta* **2015**, *155*, 23−28.
(25) Rui, X.; Sun, W.; Wu, C.; Yu, Y.; Yan, Q. An advanced sodium-ion battery composed of carbon coated $Na_3V_2(PO_4)_3$ in a porous graphene network. *Adv. Mater.* **2015**, *27*, 6670−6676.
(26) Gu, E.; Xu, J.; Du, Y.; Ge, X.; Zhu, X.; Bao, J.; Zhou, X. Understanding the influence of different carbon matrix on the electrochemical performance of $Na_3V_2(PO_4)_3$ cathode for sodium-ion batteries. *J. Alloys Compd.* **2019**, *788*, 240−247.
(27) Liu, J.; Wang, J.; Xu, C.; Jiang, H.; Li, C.; Zhang, L.; Lin, J.; Shen, Z. X. Advanced energy storage devices: Basic principles, analytical methods, and rational materials design. *Adv. Sci.* **2018**, *5*, No. 1700322.
(28) Chao, D.; Liang, P.; Chen, Z.; Bai, L.; Shen, H.; Liu, X.; Xia, X.; Zhao, Y.; Savilov, S. V.; Lin, J.; Shen, Z. X. Pseudocapacitive Na-ion storage boosts high rate and areal capacity of self-branched 2D layered metal chalcogenide nanoarrays. *ACS Nano* **2016**, *10*, 10211−10219.
(29) Raj, K. A.; Panda, M. R.; Dutta, D. P.; Mitra, S. Bio-derived mesoporous disordered carbon: An excellent anode in sodium-ion battery and full-cell lab prototype. *Carbon* **2019**, *143*, 402−412.

https://doi.org/10.1021/acsomega.2c06261
ACS Omega 2022, 7, 48192−48201